

Dual-Decoder Consistency via Pseudo-Labels Guided Data Augmentation for Semi-Supervised Medical Image Segmentation

Yuanbin Chen, Tao Wang, Hui Tang, Longxuan Zhao, Ruige Zong, Shun Chen, Tao Tan, Xinlin Zhang, and Tong Tong

Abstract—Though supervised learning gains impressive success, the acquisition of indispensable large-scale labeled datasets are often impractical in biomedical imaging partially due to expensive costs and lengthy annotations done by experienced radiologists. Semi-supervised learning has been shown to be an effective way to address this limitation by leveraging useful information from unlabeled datasets. In this paper, we present a new semi-supervised learning method referred to as Dual-Decoder Consistency via Pseudo-Labels Guided Data Augmentation (DCPA) for medical image segmentation. We devise a consistency regularization to improve the semi-supervised learning. Specifically, to promote consistent representations during the training process, we use different decoders for student and teachers networks while maintain the same encoder. Moreover, to learn from unlabeled data, we create pseudo-labels generated by the teacher networks and augment the training data with the pseudo-labels. The two techniques contribute to the improved performance of the proposed method. We evaluate the performance of the proposed method on three representative medical image segmentation datasets. Extensive comparisons to the state-of-the-art medical image segmentation methods were carried out under typical scenarios with 10% and 20% labeled data. Experimental outcomes demonstrate that our method consistently outperforms state-of-the-art semi-supervised medical image segmentation methods over the three semi-supervised settings. Furthermore, to explore the performance of proposed method under extreme condition, we conduct experiments with only 5% labeled data. The results further verify the superior performance of the proposed method. Source code is publicly online at <https://github.com/BinYcn/DCPA.git>.

Index Terms—Semi-supervised learning, consistency regularization, Pseudo-labels, Medical image segmentation.

I. INTRODUCTION

IMAGE segmentation plays a crucial and indispensable role in medical image analysis. It annotates structures of interest in medical images, e.g., computerized tomography (CT) or magnetic resonance imaging (MRI), which is beneficial to monitoring and diagnosis of diseases. Deep learning has witnessed remarkable advancements in boosting medical image segmentation. Among various deep learning based methods, convolutional neural network (CNN) methods yield cutting-edge performance and have been widely adopted. For instance, fully convolutional networks (FCNs) [1] and encoder-decoder networks (e.g., U-Net [2] and V-Net [3]) were successively proposed for this task. The success of these methods deeply rely on high-quality annotated datasets. However, it is often impractical to obtain large-scale labeled datasets in medical imaging due to expensive costs and the lengthy annotations done by only experienced radiologists.

Semi-supervised learning is an effective way to address the demanding for numerous labeled data in supervised learning while maintaining promising segmentation accuracy. This kind of methods harness useful information from a plethora of unlabeled data to improve the segmentation accuracy and have become emerging methods in medical image segmentation [4]. One of the critical research problems in semi-supervised learning is developing effective strategies for supervising unlabeled data, which already gives rise to a plethora of methods that adeptly exploit the latent potential of unlabeled data. Semi-supervised methods can be primarily classified into three distinct categories: (1) Consistency regularization methods [5]–[7], which induce the model to exhibit consistent output distributions when subjected to input perturbations. By subjecting the unlabeled data to diverse perturbations or employing augmentation techniques, the model is compelled to generate coherent predictions, thereby augmenting its generalization capability. (2) Entropy minimization methods [8]–[10], which are grounded in the clustering assumption, actively encourage the model to make confident predictions on unlabeled data. Through the minimization of entropy in the predicted probability distribution, the model acquires an increased degree of certainty, consequently fortifying its learning effectiveness. (3) Pseudo-labeling methods [11]–[13], serving

This work was supported by National Natural Science Foundation of China under Grant 62171133, in part by the Artificial Intelligence and Economy Integration Platform of Fujian Province, the Fujian Health Commission under Grant 2022ZD01003, and the Guiding Projects of Fujian Provincial Technology Research and Development Program under Grant 2022Y0023. (Corresponding author: Xinlin Zhang, Tong Tong.)

This work was supported by National Natural Science Foundation of China under Grant 62171133, in part by the Artificial Intelligence and Economy Integration Platform of Fujian Province, and the Fujian Health Commission under Grant 2022ZD01003. (Corresponding author: Xinlin Zhang, Tong Tong.)

Yuanbin Chen, Tao Wang, Hui Tang, Longxuan Zhao, Ruige Zong, Xinlin Zhang, TongTong are with the College of Physics and Information Engineering, Fuzhou University, Fuzhou 350116, China, and also with the Fujian Key Lab of Medical Instrumentation & Pharmaceutical Technology, Fuzhou University, Fuzhou 350116, China (e-mail: binycn904363330@gmail.com, ortonwangtao@gmail.com, yeahelana@gmail.com, zlx1154692412@gmail.com, zongruige@gmail.com, xinlin1219@gmail.com, ttravelong@gmail.com).

Shun Chen is with the Department of Department of Ultrasound, Fujian Medical University Union Hospital, Fuzhou, China, and also with the Fujian Medical Ultrasound Research Institute, Fuzhou, China (e-mail: shunzifjmu@126.com).

Tao Tan is with the Department of the Faculty of Applied Science, Macao Polytechnic University, Macao, 999078, China (e-mail: taotanjs@gmail.com).

as a mechanism to enrich the training set, enhance model performance by generating pseudo-labels from the unlabeled data.

Though achieving promising performance in medical image segmentation, semi-supervised learning methods face several challenges [14]. For instance, given varying advantages and limitations of different methods, it is a crucial task in selecting an appropriate method and/or an effective regularization. Moreover, the availability of a large amount of unlabeled data may cause imbalance during the learning process, biasing models towards unlabeled data. Failure in handling the imbalance between labeled and unlabeled data may degrade the performance of semi-supervised learning methods. The complex and diverse characteristics in medical images, e.g., intensity variations among imaging modalities, result in difficulties in capturing underlying patterns and generalization across different datasets. Given these limitations, developing robust semi-supervised learning methods remains a challenging but important research problem.

In this paper, we address the challenges of medical image segmentation by introducing a semi-supervised learning technique, the Dual-Decoder Consistency via Pseudo-Labels Guided Data Augmentation (DCPA). This approach is developed to fully learn information from both labeled and unlabeled data. It seeks to enhance the efficacy of unlabeled regions through two pivotal mechanisms. The first one is the Pseudo-Label generation and guided data augmentation. The teacher model within the DCPA framework is entrusted with the generation of pseudo-labels for the unlabeled dataset. Subsequent to this generation, a sophisticated data augmentation process is employed, amalgamating unlabeled data with its labeled counterpart using the Mixup technique [15]. This procedure not only augments the dataset's richness but also ensures that the generated pseudo-labels serve as the definitive labels for the mixed dataset. The second one is the consistency via Dual-Decoders. The architecture of the DCPA encompasses both teacher and student models, each fortified with a shared encoder and dual-decoders, each possessing distinct operational strategies. To ensure the reliability and consistency of the model's predictions, the outputs of the student model's dual-decoders are harmonized through meticulously designed consistency constraints.

The main contributions of this paper are as follows:

- We introduce a novel semi-supervised medical image segmentation paradigm, integrating pseudo-labels and consistency. This innovative approach adeptly harnesses the latent potential of unlabeled data, manifesting in significant enhancements in semi-supervised image segmentation efficacy.
- We propose a novel dual-decoder network, underpinned by the mean-teacher model. The integration of a consistency scheme steers the model's training trajectory, facilitating the extraction of holistic and universal feature representations.
- We performed comprehensive evaluations of the proposed method on three challenging public medical image segmentation benchmarks. The experimental results demonstrate the superiority of the proposed method, as

it outperforms the performance of the state-of-the-art methods.

II. RELATED WORK

A. Supervised medical image segmentation

The superior learning capability of deep learning has inspired a fruitful of supervised learning based medical image segmentation methods [1]–[3], [15]–[21]. In general, those methods gain improved performance via data augmentation, optimized network architecture, and improved loss functions. Specifically, data augmentation has been empirically shown to be a simple yet effective technique in enhancing performance and robustness [17]. Mixup [15] is one of the data augmentation techniques that enriches the diversity of the dataset through the generating interpolated samples. Many other works centered on optimizing network architectures to improve performance. For instance, CE-Net [18] utilizes a dense atrous convolution module and an residual multi-kernel pooling module to learn advanced features and retain additional spatial information. The introduction of Transformer models [22] to obtain exceptional capacity for modeling global context. Swin-Unet [20] employs a layered Swin Transformer [19] with shifted windows as an encoder, enabling the extraction of contextual features. The loss function plays an indispensable role in deep learning methods. Research works in improving loss functions can be categorized into three types: (1) distribution-based losses, such as cross-entropy loss [2], which aim to maximize the similarity between predictions and true labels in the distribution space; (2) region-based losses, such as Dice loss [3], which strive to minimize the discrepancy between predictions and true labels; (3) distance-based losses, such as boundary loss [21], which aim to minimize the boundary distance between predictions and true labels in Euclidean distance space. Supervised learning based medical image segmentation methods obtain impressive performance, but requires large amount of manually labeled data for training.

B. Semi-supervised medical image segmentation

Semi-supervised learning has gained prominence as an effective approach to mitigate the challenges associated with acquiring large-scale labeled data, especially in the realm of medical image segmentation. To optimally leverage information from unlabeled data, numerous techniques grounded in diverse principles have been proposed by researchers. A prevalent strategy involves the use of consistency regularization. Here, the model is trained to maintain consistency in its predictions across varied tasks or representations [23]–[25]. This consistency is also emphasized when minor perturbations, such as noise or data augmentations, are introduced to the input [6], [26], [27]. For instance, TCSM-V2 [27] incorporated multiple data and model perturbations—including flipping, rotation, resizing, noise addition, and dropout—within the mean-teacher framework [6] to ensure consistent model predictions across different input variations. Additionally, Li et al. [23] utilized a multi-task network structure tailored for image segmentation and signed distance map regression, integrating shape and position priors. They incorporated a discriminator

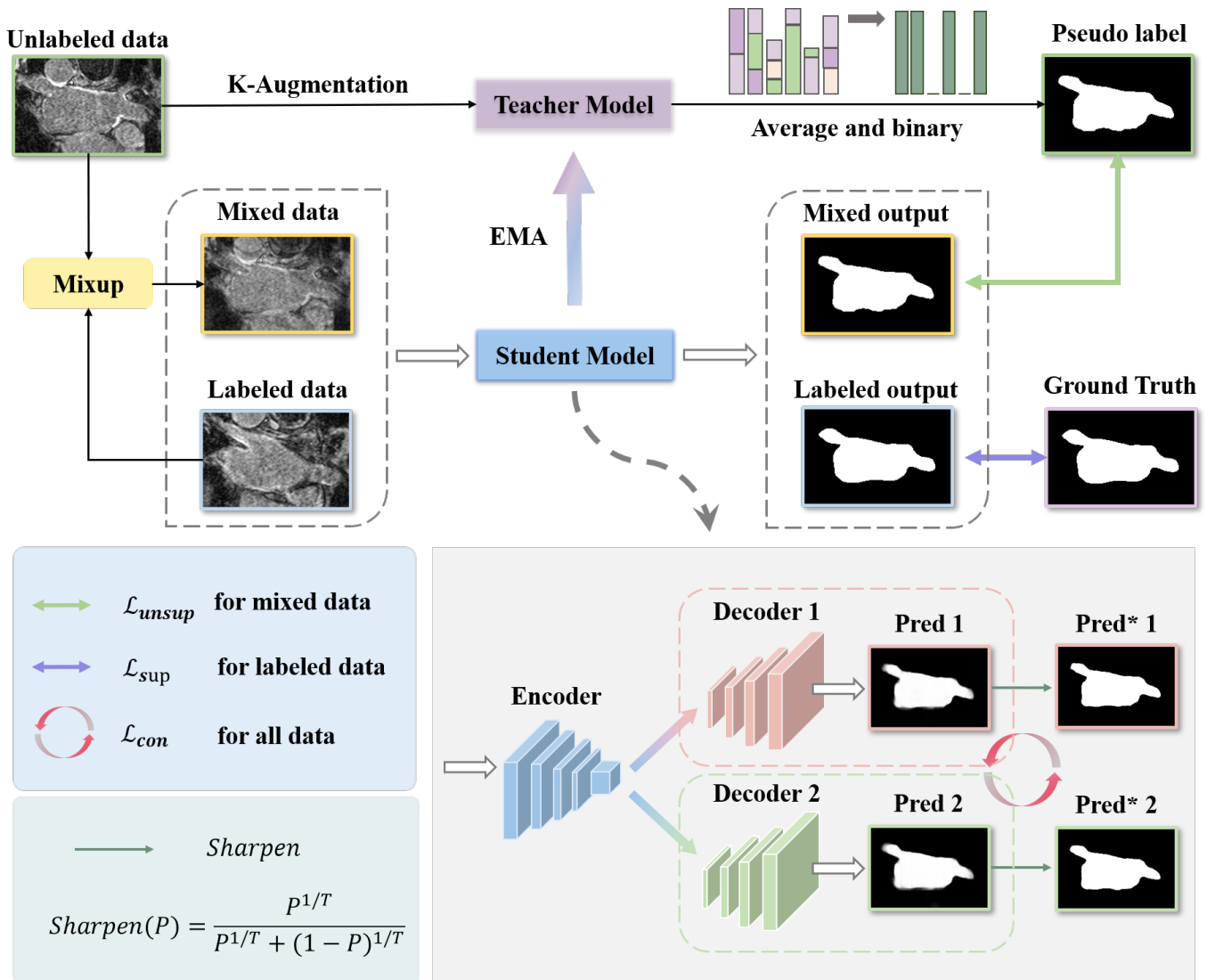


Fig. 1. Overview of the proposed DCPA method. Detailed descriptions of both the teacher model and the student model are provided beneath the figure. Notably, Decoder 1 and Decoder 2 correspond to two distinct decoders employing different upsampling strategies. The circular annotations of L_{con} indicate the computation of consistency loss between Pred 1 and Pred* 2, as well as between Pred 2 and Pred* 1. EMA stands for exponential moving average.

as a regularization component, enhancing the stability and robustness of segmentation outcomes. Another widely adopted approach is entropy minimization, which prompts the model to produce confident predictions for unlabeled data by reducing the entropy of the model's output probability distribution [28], [29]. For example, Hang et al. [28] integrated entropy minimization into the student network, enabling it to generate confident predictions for unlabeled images. Another type of methods are based on the pseudo label techniques. These methods generate pseudo-labels for unlabeled data, guiding the model's learning trajectory. Wang et al. [30] proposed the integration of a trust module to reassess pseudo-labels derived from model outputs, setting a threshold to cherry-pick high-confidence predictions. Meanwhile, Li et al. [31] unveiled a self-ensembling strategy that employs Exponential Moving Average (EMA) to yield precise and dependable predictions, addressing challenges linked with noisy and fluctuating pseudo-labels.

The previously mentioned methods have drawbacks. Some require complex network structures and additional training components, increasing computational and resource demands. Others show suboptimal performance with noisy or uncertain pseudo-labeling, leading to instability or performance decline. In response to these challenges and limitations, we have introduced a new method building upon previous work. It incorporates pseudo-labels, consistency regularization, and data augmentation within a model based on the mean-teacher framework for semi-supervised medical image segmentation, which is both straightforward and highly effective.

III. METHOD

To provide a clear and precise representation of the proposed method, we introduce the following notations. We partition the training dataset into two subsets: a labeled set, D_L^N , with N samples, and an unlabeled set, D_U^M , with M samples. For an image $x_i \in D_L^N$, its corresponding ground truth label y_i is

known. However, for an image $x_i \in D_U^M$, the ground truth label is absent. Thus, the datasets are defined as:

$$\begin{aligned} D_L^N &= \{x_l^i, y_l^i | i = 1, \dots, N\}, \\ D_U^M &= \{x_u^i | i = 1, \dots, M\}. \end{aligned}$$

The probability map generated for x is represented by $p(y_{pred}|x; \theta)$, where θ signifies the parameters of the segmentation model $f(\theta)$.

A. Model architecture

In this paper, we introduce a novel semi-supervised medical image segmentation method, referred to as DCPA, as illustrated in Fig. 1. The DCPA framework is built upon two core components which can fully use both labeled and unlabeled data. The first component focuses on data augmentation. We harness the potential of unlabeled data by generating pseudo-labels. To further enhance the training dataset, we employ Mixup, an effective augmentation technique, which merges these pseudo-labeled data with the original labeled samples. This augmented dataset then serves as the foundation for the subsequent training phase. The second component revolves around the architecture and training of the student and teacher models. Both models share a consistent structure, featuring a unified encoder and a dual-decoder, each equipped with distinct up-sampling strategies. However, they differ in the training strategies. The student model is trained using our proposed loss function, while the teacher model, in contrast, adopts the Exponential Moving Average (EMA) approach, adjusting the weights based on the student model's performance.

Subsequent sections detail the two components of our methodology.

B. Pseudo-Labels Guided Data Augmentation

1) *Pseudo-Labels Generation*: The weak data augmentation techniques, such as random perturbations, are firstly applied to our dataset. This augmentation is applied differently for labeled and unlabeled images. For every batch of labeled images, denoted as $X_L^b \in D_L^N$, we generate a single augmented version, represented as $\hat{X}_L^b = Augment(X_L^b)$. In contrast, for each batch of unlabeled images $X_U^b \in D_U^M$, we produce K augmented versions, given by $\hat{X}_U^{b,k} = Augment(X_U^b)$ for $k \in \{1, \dots, K\}$.

Once the data is augmented, we employ the teacher model to compute the average predicted segmentation distribution, \bar{P}^b , from the augmented unlabeled samples. This average distribution is then subjected to a binary operation to generate the pseudo-labels, P^b . The binary operation is conducted based on a threshold, H , which is commonly set to 0.5. The specific computational formulas are:

$$\bar{P}^b = \frac{1}{K} \sum_{k=1}^K p(y_{pred} | \hat{X}_U^{b,k}; \theta_t), \quad (1)$$

$$P^b(x, y) = \begin{cases} 1, & \text{if } \bar{P}^b(x, y) \geq H, \\ 0, & \text{otherwise.} \end{cases} \quad (2)$$

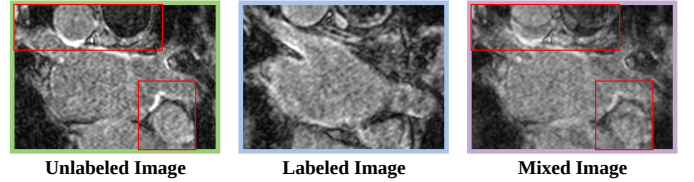


Fig. 2. Illustration of the effects of Mixup. The red rectangles within the image highlight areas where noticeable alterations are observed before and after applying Mixup.

where, θ_t represents the parameters of the teacher model, and $P^b(x, y)$ denotes the pixel value at the coordinate (x, y) within the pseudo-labels. If the pixel value in \bar{P}^b meets or exceeds the threshold H , its corresponding value in P^b is assigned as 1; otherwise, it remains 0. These pseudo-labels, P^b , are subsequently integrated into the unsupervised loss term.

2) *Data Augmentation with Mixup*: Drawing inspiration from Mixmatch [9], we incorporate Mixup [15] to combine augmented unlabeled images with augmented labeled images. This fusion enhances data diversity through augmentation. Given a pair of images, x_1 and x_2 , the resultant mixed image, x' , is formulated as:

$$\lambda \sim Random(Beta(\alpha, \alpha)), \quad (3)$$

$$\lambda' = Max(\lambda, 1 - \lambda), \quad (4)$$

$$x' = \lambda' x_1 + (1 - \lambda') x_2, \quad (5)$$

where α is a hyperparameter, and *Beta* denotes the Beta distribution. Note that we do not apply Mixup [15] to labeled images due to the inherent complexities of medical images, which often exhibit significant variations in morphology, size, and anatomical positioning.

Fig. 2 shows the results of applying Mixup [15] to a pair of images. Post-Mixup, the resultant image predominantly retains the semantic essence of the unlabeled data. However, the inclusion of labeled data introduces subtle modifications, especially in areas highlighted by the red rectangle. Despite these alterations, the core semantic information remains largely intact. Thus, we designate the pseudo-labels P^b as the label for the mixed image.

To streamline the Mixup process, we initiate by shuffling the augmented labeled images, \hat{X}_L^b , to form set W^b . Subsequently, Mixup is applied to merge the augmented unlabeled images, $\hat{X}_U^{b,k}$, with set W^b , culminating in the creation of mixed images $M^{b,k}$. These mixed images are then paired with pseudo-labels P^b to produce the mixed data D_M . The corresponding formulas are:

$$W^b = Shuffle(\hat{X}_L^b), \quad (6)$$

$$M^{b,k} = (Mixup(\hat{X}_U^{b,k}, W_{i \% |\hat{X}_L^b|}^b); i \in (1, \dots, |\hat{X}_U^{b,k}|)), \quad (7)$$

$$D_M = ((M^{b,k}, P^b); b \in (1, \dots, B), k \in (1, \dots, K)), \quad (8)$$

where the symbol $\%$ signifies the modulo operation.

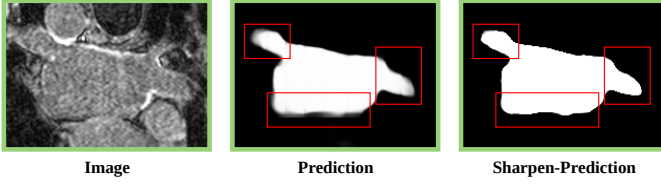


Fig. 3. Demonstration of results after post-sharpening. The red rectangles spotlight regions with pronounced alterations pre and post-sharpening.

C. Dual-Decoder Consistency

1) *Dual-Decoder architecture based on the mean-teacher framework*: Fig. 1 illustrates the architecture of both the student and teacher models, which are constructed upon the V-Net backbone. This design comprises a shared encoder and a dual-decoder, each with distinct strategies: the transposed convolutional layer and the linear interpolation layer. The purpose of this dual-decoder approach is to exploit the differences between the decoder outputs, thereby capturing and representing the model’s inherent uncertainty.

To enhance the quality of pseudo-labels derived from unlabeled data, we adopt the Exponential Moving Average (EMA) approach. This method updates the teacher model’s parameters based on the student model’s parameters, integrating historical states throughout the learning trajectory. The effectiveness of this approach is supported by [6]. The update rule for the teacher model’s parameters at a given time step, represented as θ'_t , is:

$$\theta'_t = \alpha\theta'_{t-1} + (1 - \alpha)\theta_t, \quad (9)$$

where θ'_{t-1} denotes the teacher model’s historical parameters, while θ_t represents the student model’s current parameters. The hyperparameter α serves as a smoothing coefficient, balancing the relationship between the teacher and student models.

2) *Sharpening function*: To maximize the utility of unlabeled data, we introduce a sharpening function. This function aims to reduce the entropy of the probability maps generated by the student model, resulting in soft-pseudo-labels $Pred_i^*$:

$$Pred_i^* = \frac{Pred_i^{\frac{1}{T}}}{Pred_i^{\frac{1}{T}} + (1 - Pred_i)^{\frac{1}{T}}}, i \in (1, 2), \quad (10)$$

where the hyperparameter T controls the sharpening temperature. As T approaches zero, the output of $Pred_i^*$ converges to a Dirac (“one-hot”) distribution, prompting the model to yield predictions with diminished entropy. The sharpening operation’s impact is shown in Fig. 3, where segmentation boundaries are accentuated and image blurriness is reduced, especially in regions delineated by the red rectangle.

Building upon the sharpening process, we then employ the derived soft-pseudo-labels $Pred_1^*$ and $Pred_2^*$ to supervise the probability maps $Pred_2$ and $Pred_1$, respectively. This step enforces a consistency constraint, bridging the gap between decoder outputs and guiding the model’s learning direction.

IV. EXPERIMENTS

In this section, three representative medical image datasets were utilized to extensively evaluate the performance and effectiveness of the proposed method.

A. Dataset and Preprocessing

1) *Pancreas-CT dataset*: The pancreas-CT dataset [32] used in this study was obtained from the National Institutes of Health Clinical Center. It consists of 82 3D abdominal contrast-enhanced CT scans acquired using Philips and Siemens MDCT scanners. The scans have a fixed in-plane resolution of 512×512 and varying intra-slice spacing ranging from 1.5 to 2.5 mm. The voxel value clipping operation [24] were utilized to ensure a range of $[-125, 275]$ Hounsfield Units (HU). Subsequently, the data was further resampled to achieve an isotropic resolution of $1.0 \times 1.0 \times 1.0$ mm. Similar to [25], [29], we select 62 samples as the training set and 20 samples as the testing set.

2) *LA dataset*: The LA (Left Atrium) dataset [33], a benchmark dataset for the 2018 Atrial Segmentation Challenge, comprises 154 gadolinium-enhanced MR scans with an isotropic resolution of $0.625 \times 0.625 \times 0.625$ mm³. Since this dataset does not provide labels for its test set, in this study we used only its labeled samples (a total of 100). Specifically, 80 samples were used as the training set and 20 samples were used for the testing set.

3) *ACDC dataset*: The ACDC (Automated Cardiac Diagnosis Challenge) dataset [34] was collected from real clinical exams conducted at the University Hospital of Dijon. This dataset consists of cardiac MR imaging samples obtained from 100 patients, specifically multi-slice 2D cine MRI, which were used for training. Following the existing work [24], we selected 70 samples as the training set, 10 samples as the validation set and 20 samples as the testing set.

B. Implementation Details

1) *3D Segmentation*: The typical image preprocessing techniques [24], [26], [29], e.g., cropping, normalization, and unit variance were performed to the images before the neural networks. Due to the computational demands associated with 3D training, a patch-based approach was employed during the training phase, where the training data was divided into small patches. Specifically, a patch size of $112 \times 112 \times 80$ was used for the LA dataset while a patch size of $96 \times 96 \times 96$ was used for the pancreas-CT dataset. Moreover, data augmentation techniques such as 2D rotation and flip operations were applied to augment the LA dataset.

For semi-supervised learning experiments, a subset of training data were used as the labeled training set while the rest act as the unlabeled training set. Specifically, we consider three different settings, i.e., training with 5%, 10%, and 20% labeled data, respectively. An unusual setting with only 5% labeled data was adopted to further evaluate the performance of the proposed method under the extreme scenario. For the proposed method, we used the V-Net as the network backbone. A batch size of 4 was utilized, in which two labeled patches and two

TABLE I
COMPARISON WITH THE SOTA METHODS ON THE PANCREAS-CT DATASET.

Method	Scans used		Metrics			
	Labeled	Unlabeled	Dice(%) \uparrow	Jaccard(%) \uparrow	95HD(voxel) \downarrow	ASD(voxel) \downarrow
V-Net	3(5%)	0	29.32	19.61	43.67	15.42
V-Net	6(10%)	0	54.94	40.87	47.48	17.43
V-Net	12(20%)	0	71.52	57.68	18.12	5.41
V-Net	62(All)	0	83.48	71.99	4.44	1.26
UA-MT (MICCAI'19)			43.15	29.07	51.96	20.00
SASSNet (MICCAI'20)			41.48	27.98	47.48	18.36
DTC (AAAI'21)			47.57	33.41	44.17	15.31
URPC (MIA'22)	3(5%)	59(95%)	45.94	34.14	48.80	23.03
SS-Net (MICCAI'22)			41.39	27.65	52.12	19.37
MC-Net+ (MIA'22)			32.45	21.22	58.57	24.84
Ours			79.16	65.86	5.88	1.69
UA-MT (MICCAI'19)			66.44	52.02	17.04	3.03
SASSNet (MICCAI'20)			68.97	54.29	18.83	1.96
DTC (AAAI'21)			66.58	51.79	15.46	4.16
URPC (MIA'22)	6(10%)	56(90%)	73.53	59.44	22.57	7.85
SS-Net (MICCAI'22)			73.44	58.82	12.56	2.91
MC-Net+ (MIA'22)			70.00	55.66	16.03	3.87
Ours			81.34	68.97	5.40	1.69
UA-MT (MICCAI'19)			76.10	62.62	10.84	2.43
SASSNet (MICCAI'19)			76.39	63.17	11.06	1.42
DTC (AAAI'21)			76.27	62.82	8.70	2.20
URPC (MIA'22)	12(20%)	50(80%)	80.02	67.30	8.51	1.98
SS-Net (MICCAI'22)			78.68	65.96	9.74	1.91
MC-Net+ (MIA'22)			79.37	66.83	8.52	2.03
Ours			82.89	71.17	4.54	1.23

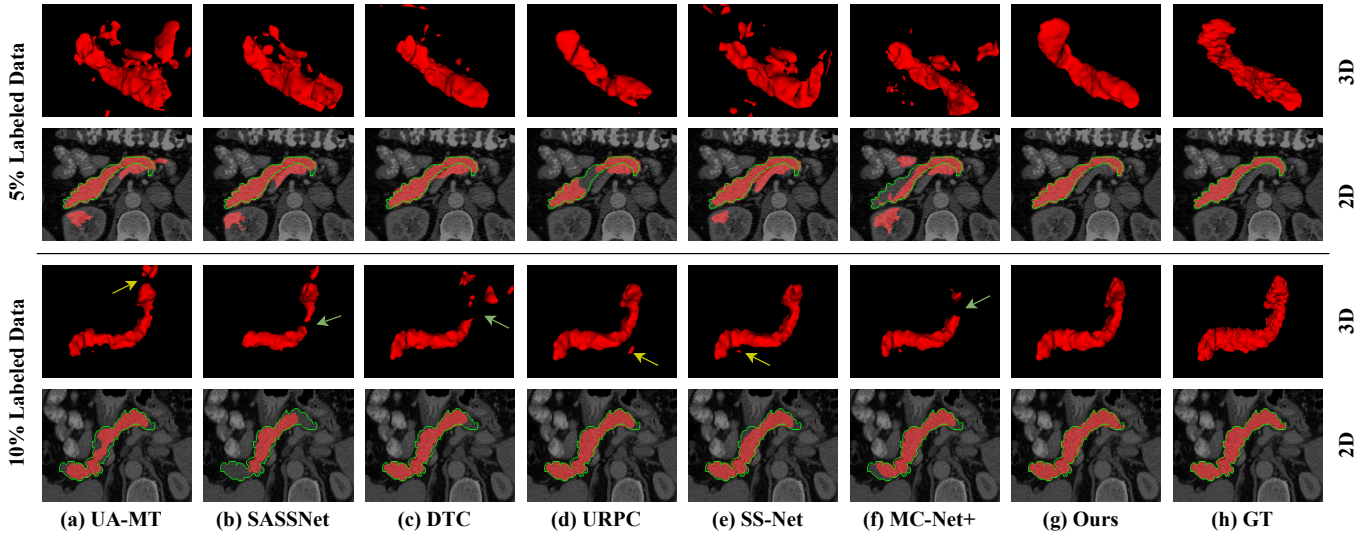


Fig. 4. 2D and 3D views of the segmentation results on the Pancreas-CT dataset. For better visualization, we delineate the segmentation outline of the ground truth (green) and overlay it over the predictions.

unlabeled patches were included. The 3D DCPA model was trained for a total of 15,000 iterations. During the inference stage, a patch-based pipeline with a sliding window strategy was employed to combine the predictions from the patches and generate the final segmentation outputs.

2) *2D Segmentation*: On the ACDC dataset, a normalization was carried out to achieve a zero mean and unit variance for the samples. Additionally, to enhance dataset diversity, data were augmented by randomly applying rotations and

flips. Similar to the 3D segmentation experiments, a subset of training data was randomly selected as the labeled training set while the rest act as the unlabeled training set. Specifically, three different settings were used for evaluation, i.e., training with 5%, 10%, and 20% labeled data, respectively. An unusual setting with only 5% labeled data was adopted to further evaluate the performance of the proposed method under the extreme scenario.

Here our 2D DCPA model employed the U-Net architecture

TABLE II
COMPARISON WITH THE SOTA METHODS ON THE LA DATASET.

Method	Scans used		Metrics			
	Labeled	Unlabeled	Dice(%) \uparrow	Jaccard(%) \uparrow	95HD(voxel) \downarrow	ASD(voxel) \downarrow
V-Net	4(5%)	0	52.55	39.60	47.05	9.87
V-Net	8(10%)	0	78.57	66.96	21.20	6.07
V-Net	16(20%)	0	86.96	77.31	11.85	3.22
V-Net	80(All)	0	91.71	84.76	5.57	1.59
UA-MT (MICCAI'19)			82.26	70.98	13.71	3.82
SASSNet (MICCAI'19)			81.60	69.63	16.60	3.58
DTC (AAAI'21)			81.25	69.33	14.90	3.99
URPC (MIA'22)	4(5%)	76(95%)	82.48	71.35	14.65	3.65
SS-Net (MICCAI'22)			86.33	76.15	9.97	2.31
MC-Net+ (MIA'22)			82.07	70.38	20.49	5.72
Ours			89.34	80.79	8.13	1.69
UA-MT (MICCAI'19)			86.28	76.11	18.71	4.63
SASSNet (MICCAI'19)			85.22	75.09	11.18	2.89
DTC (AAAI'21)			87.51	78.17	8.23	2.36
URPC (MIA'22)	8(10%)	72(90%)	85.01	74.36	15.37	3.96
SS-Net (MICCAI'22)			88.43	79.43	7.95	2.55
MC-Net+ (MIA'22)			88.96	80.25	7.93	1.86
Ours			90.91	83.39	5.53	1.65
UA-MT (MICCAI'19)			88.74	79.94	8.39	2.32
SASSNet (MICCAI'19)			89.16	80.60	8.95	2.26
DTC (AAAI'21)			89.52	81.22	7.07	1.96
URPC (MIA'22)	16(20%)	64(80%)	88.74	79.93	12.73	3.66
SS-Net (MICCAI'22)			89.86	81.70	7.01	1.87
MC-Net+ (MIA'22)			91.07	83.67	5.84	1.99
Ours			91.64	84.63	5.04	1.52

as its backbone. A patch-based training was used, in which we randomly extracted 2D patches with a dimension of 256×256 . A batch size of 24 was used, in which 12 labeled data and 12 unlabeled samples were included. The model was trained for a total of 30,000 iterations to optimize its performance. It is worth noting that all experimental configurations on the ACDC dataset adhered to the guidelines set by the public benchmark established by [35], ensuring fair comparisons with other methods.

3) *Experimental settings*: All experiments were performed on a server equipped with an NVIDIA GeForce RTX 3090 24GB GPU running Ubuntu 20.04 and PyTorch 1.12.1. To optimize the segmentation tasks, we employed an SGD optimizer with a momentum of 0.9 and weight decay of 0.0001. The initial learning rate was set to 0.01. Regarding the hyperparameter settings, K was defined as 2, T was set to 0.1, H was established as 0.5, and α was assigned a value of 0.75 for all tasks. In addition, morphological operation was used to enhance the segmented outcomes, such as opting for the largest connected component as the post-processing module [23], [35]. Four metrics were used for evaluation: Dice, Jaccard, the 95% Hausdorff Distance (95HD), and average surface distance (ASD).

C. Experimental results

To fully assess the effectiveness of our proposed method, we conducted comparisons with both supervised and semi-supervised methods, including V-Net [3], UA-MT [26], SASS-Net [23], DTC [24], URPC [25], SS-Net [35], and MC-Net+

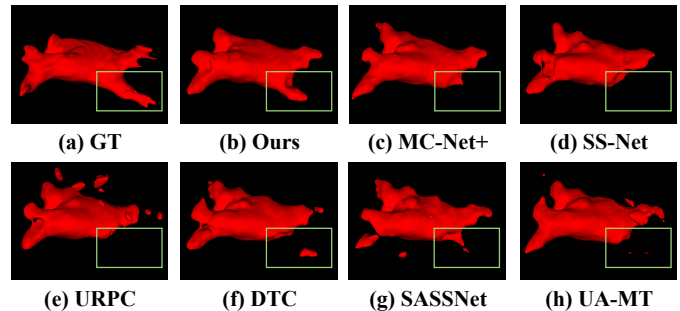


Fig. 5. 3D views of the segmentation results by different methods on the LA dataset. Note that 5% labeled data were used for training.

[29]. Note that V-Net [3] is the supervised learning method while the others are semi-supervised methods. To facilitate fair comparisons, we trained the supervised learning method, i.e., V-Net, with varying a amount of labeled data from 5% to 100%.

1) *Results on the Pancreas-CT dataset*: Table I presents quantitative results for the Pancreas-CT dataset. Evidently, the proposed method significantly outperforms all other semi-supervised methods across all quantitative metrics. The proposed DCPA greatly enhances the Dice score from 29.32% to 79.16% with only 5% labeled data, representing a notable performance improvement compared to the fully-supervised method. Similarly, when utilizing 10% labeled data, DCPA achieves a Dice score surpassing that of other cutting-edge semi-supervised methods trained with 20% labeled data. The

TABLE III
COMPARISON WITH THE SOTA METHODS ON THE ACDC DATASET.

Method	Scans used		Metrics			
	Labeled	Unlabeled	Dice(%) \uparrow	Jaccard(%) \uparrow	95HD(voxel) \downarrow	ASD(voxel) \downarrow
U-Net	3(5%)	0	47.83	37.01	31.16	12.62
U-Net	7(10%)	0	77.34	66.20	9.18	2.45
U-Net	14(20%)	0	85.15	75.48	6.20	2.12
U-Net	70(All)	0	91.65	84.93	1.89	0.56
UA-MT (MICCAI'19)			50.04	39.57	29.31	9.88
SASSNet (MICCAI'19)			57.77	46.14	20.05	6.06
DTC (AAAI'21)			56.90	45.67	23.36	7.39
URPC (MIA'22)	3(5%)	67(95%)	55.87	44.64	13.60	3.74
SS-Net (MICCAI'22)			65.82	55.38	6.67	2.28
MC-Net+ (MIA'22)			64.77	54.06	12.39	3.45
Ours			85.86	76.13	5.83	2.03
UA-MT (MICCAI'19)			81.58	70.48	12.35	3.62
SASSNet (MICCAI'19)			84.14	74.09	5.03	1.40
DTC (AAAI'21)			82.71	72.14	11.35	2.99
URPC (MIA'22)	7(10%)	63(90%)	81.77	70.85	5.04	1.41
SS-Net (MICCAI'22)			86.78	77.67	6.07	1.40
MC-Net+ (MIA'22)			87.10	78.06	6.68	2.00
Ours			88.10	79.45	1.86	0.57
UA-MT (MICCAI'19)			85.87	76.78	5.06	1.54
SASSNet (MICCAI'19)			87.04	78.13	7.84	2.15
DTC (AAAI'21)			86.28	77.03	6.14	2.11
URPC (MIA'22)	14(20%)	56(80%)	85.07	75.61	6.26	1.77
SS-Net (MICCAI'22)			88.10	79.70	3.34	0.95
MC-Net+ (MIA'22)			88.51	80.19	5.35	1.54
Ours			89.19	81.08	1.71	0.46

proposed method achieves quantitative results comparable to the upper bound (V-Net with 100% labeled training data) even when employing only 20% labeled data for training. These results vividly demonstrate the effectiveness of the proposed method in leveraging information from unlabeled data to enhance segmentation performance.

The segmentation results, when visualized, further verify our proposed method's enhanced performance compared to other semi-supervised techniques. Fig. 4 presents the segmentation outcomes derived from various methods. Notably, in both scenarios (with 5% and 10% labeled data), our method produces segmentation results that closely align with the ground truth. In contrast, competing methods tend to exhibit irregularities or false positives.

2) *Results on the LA dataset:* Our comparisons were extended to encompass an additional 3D dataset, enhancing the assessment of the effectiveness and generalization of our proposed method. Table II presents the quantitative results. In all semi-supervised settings, the proposed DCPA surpasses other state-of-the-art semi-supervised methods in terms of quantitative metrics. Impressively, even when trained with only 20% labeled data, our method produces results nearly comparable to the upper bound established by V-Net, which is trained with a full 100% labeled dataset. In addition to the numerical outcomes, the segmentation visualizations in Fig. 5 underscore the superior performance of our approach. In the highlighted area within Fig. 5, it becomes evident that when using only 5% of annotated data, the other models exhibit significant instances of missed detections. In contrast, our model offers a more comprehensive representation of the left

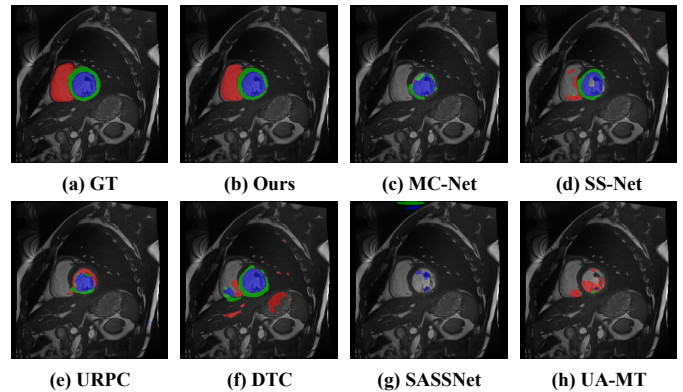


Fig. 6. Segmentation results of different method on the 2D ACDC dataset with a 5% labeled data. The left ventricle, myocardium, and right ventricle are distinctly color-coded as red, green, and blue, respectively.

atrium and preserves finer details.

3) *Results on the ACDC dataset:* The proposed method was further extended to address 2D multi-class segmentation tasks. Quantitative metrics were averaged across three classes: the myocardium, left ventricle, and right ventricle, and the results are presented in Table III. The results demonstrate that in various semi-supervised settings, the proposed method consistently ranks at the top across Dice, Jaccard, 95HD, and ASD metrics, outperforming competing semi-supervised methods. Regardless of the percentage of labeled data used, the proposed method consistently achieves a Dice score above 85.00%, affirming its stability and efficacy. Moreover, the

TABLE IV
ABLATION RESULTS THE PANCREAS-CT DATASET TO EVALUATE THE CONTRIBUTION OF EACH COMPONENT OF THE PROPOSED METHOD.

Scans used		Method				Metrics			
Labeled	Unlabeled	DD	PL	MT	Mixup	Dice(%)	Jaccard(%)	95HD(voxel)	ASD(voxel)
3(5%)	59(95%)					29.32	19.61	43.67	15.42
		✓				36.77	24.47	46.34	16.41
		✓	✓			44.55	30.55	55.97	21.20
		✓	✓	✓		62.65	47.59	34.57	12.08
		✓	✓		✓	69.07	53.64	26.08	7.55
		✓	✓	✓	✓	79.16	65.86	5.88	1.69
6(10%)	56(90%)					54.94	40.87	47.48	17.43
		✓				66.56	52.10	16.80	2.32
		✓	✓			71.12	56.41	37.71	11.52
		✓	✓	✓		79.38	66.47	6.83	1.73
		✓	✓		✓	78.02	64.44	9.61	3.02
		✓	✓	✓	✓	81.34	68.97	5.40	1.69
12(20%)	50(80%)					71.52	57.68	18.12	5.41
		✓				76.74	63.64	9.52	2.58
		✓	✓			79.17	66.23	9.79	2.56
		✓	✓	✓		81.38	69.04	8.71	3.71
		✓	✓		✓	82.64	70.75	5.31	1.34
		✓	✓	✓	✓	82.89	71.17	4.54	1.23

”DD” denotes the dual-decoder consistency, ”PL” the pseudo-labels, and ”MT” the mean-teacher model. A check mark denotes introducing the associated component in the proposed method.

visualized results also clearly demonstrate the superior performance of the proposed method over the competing methods. As shown in Fig. 6, competing methods encounter challenges in accurately segmenting the left ventricle, and defining precise boundaries for the myocardium and right ventricle remains a challenge for several of them.

Overall, experimental results across three segmentation datasets, spanning both 2D and 3D imaging, highlight the proposed method’s superiority over current state-of-the-art competing methods. Notably, the proposed method, with just 20% labeled data, can yield results on par with the supervised learning method using a full 100% labeled data. These results indicate the proposed method’s capability in harnessing useful information from unlabeled data.

V. DISCUSSION

A. Ablation Studies

In this section, ablation studies were performed on 1) DCPA components, 2) the number of decoders N , 3) the amount of weak data augmentation on unlabeled data K , and 4) temperature T .

1) *Proposed model components*: Experiments were conducted on the Pancreas-CT dataset to evaluate the contributions of the various components of the proposed method. The quantitative results under different settings (5%, 10%, and 20% labeled data) are listed in Table IV. From the experimental results, we empirically highlight that in semi-supervised learning, each individual component distinctly contributes to performance improvements. Furthermore, the peak of performance is realized when these elements work in synergy.

2) *Number of decoders*: The impact of the number of decoders (N) on the Pancreas-CT dataset was also examined across three semi-supervised settings. In our experiments, for $N = 1$, we employed the transposed convolutional layer for

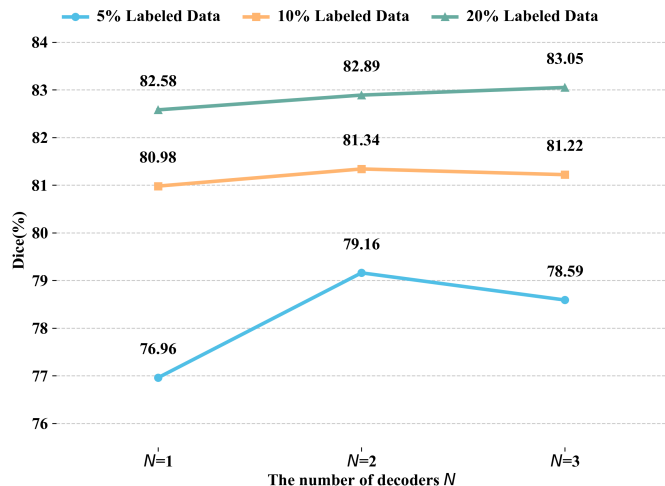


Fig. 7. Dice score variation versus the number of decoders on the Pancreas-CT dataset.

upsampling. For $N = 2$, a second decoder was introduced, using linear interpolation for upsampling. Similarly, in the vein of MC-Net+, $N = 3$ added a third decoder with nearest interpolation for upsampling. It’s worth noting that consistency losses between different decoders were incorporated for both $N = 2$ and $N = 3$. The results, illustrated in Fig. 7, show that combining consistency loss with multiple decoders can boost performance. While $N = 2$ achieves a peak performance of 83.05% with 20% labeled data, it falls in scenarios with fewer annotations and also incurs higher training costs. For optimal performance, setting $N = 2$ in the proposed method is recommended.

3) *Number of weak data augmentation*: Evaluations were performed on the Pancreas-CT dataset in three semi-supervised scenarios to analyze the influence of the number of weak data

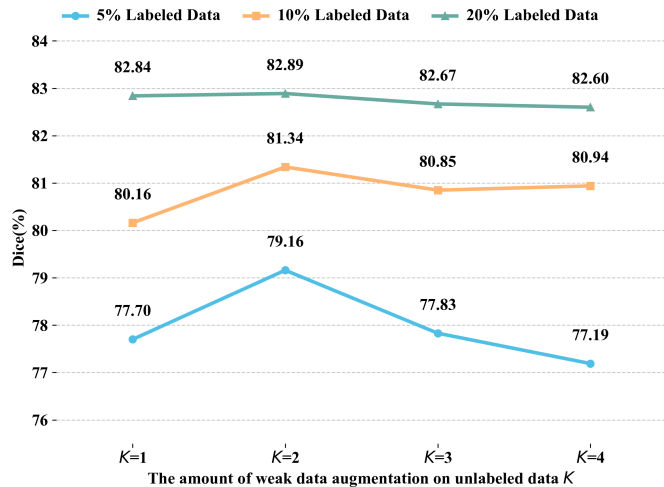


Fig. 8. Dice score versus the number of weak data augmentation on the Pancreas-CT dataset.

augmentations (K) applied to unlabeled data. For $K = 1$, the predictions of the teacher model are directly used as pseudo-labels for the unlabeled data. Otherwise, the average of the predictions of the teacher model serves as the pseudo-labels. As depicted in Fig. 8, under the 5% labeled data scenario, the performance of our proposed method exhibits heightened sensitivity to variations in K . However, as the amount of labeled data increases, the effect of altering K diminishes. Particularly, a consistent peak performance is observed with $K = 2$ across all settings. Hence, selecting $K = 2$ for network training was our choice.

4) *Sharpening temperatures*: The inclusion of a sharpening function in the proposed method is intended to improve the clarity of segmentation boundaries and reduce the presence of blurry features. Evaluations were conducted on three datasets with only 10% labeled data to evaluate the impact of the temperature coefficient, denoted as T , in the sharpening function. The results shown in Fig. 9 indicate the robustness of the proposed method to the temperature coefficient. Note that a relatively high T value makes the proposed method prone to blurry features, diminishing its effectiveness. Conversely, a relatively low T value expose yields the pitfalls of incorrect predictions. The proposed method achieves its peak performance at $T = 0.1$. Based on these observations, $T = 0.1$ was chosen as the temperature coefficient for the sharpening function.

B. Limitations and Future Works

While the proposed method allows promising results in medical image segmentation, its dual-decoder consistency has been primarily centered on exploring inter-decoder differences, with a somewhat narrow exploration of upsampling strategies. Moving forward, several interesting research directions emerge:

- **Model Disparities**: Investigating the differences between various models, such as Transformers and CNNs, might allow us to harness the unique strengths of each architecture.

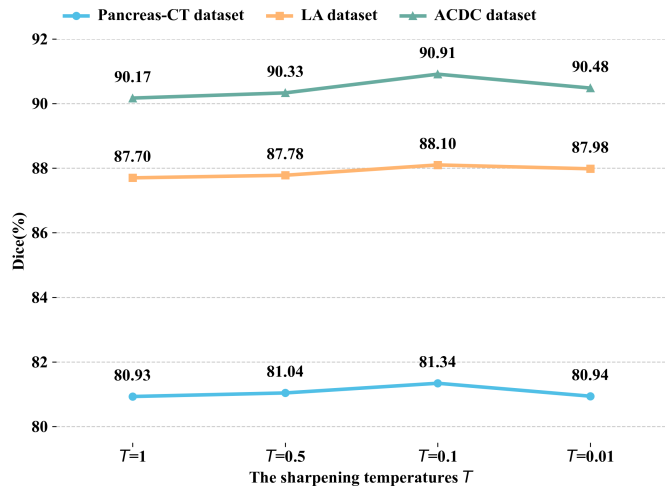


Fig. 9. Dice scores versus sharpening temperature on three datasets.

- **Synergistic Approaches**: Combining our Pseudo-Label Guided Data Augmentation method with other advanced techniques, like Generative Adversarial Networks [36] and Meta-Learning [37], can potentially enhance the performance and resilience.
- **Expanded Applicability**: Broadening the scope of our method to encompass wider medical image domains, such as semi-supervised medical image classification, could capitalize on the power of limited labeled data, especially in distinguishing between benign and malignant cases.

VI. CONCLUSION

In addressing the challenge of medical image segmentation with limited labeled data, we introduced the DCPA model, a semi-supervised approach built upon the mean-teacher framework. This model employs a dual-decoder architecture, using the teacher model’s predictions as pseudo-labels for unlabeled data. To enrich the training process, we integrated a data augmentation technique, blending labeled and unlabeled datasets. Additionally, constraints were applied during training to ensure consistent predictions between the dual-decoders.

Empirical experiments demonstrate the proposed method’s superiority, outperforming six state-of-the-art models across diverse scenarios on three public datasets. Its robust performance, especially with just 5% labeled data, highlights its potential in data-scarce medical image segmentation. This research not only demonstrates the effectiveness of the proposed method but also suggests a promising direction for future semi-supervised segmentation endeavors.

REFERENCES

- [1] J. Long, E. Shelhamer, and T. Darrell, “Fully convolutional networks for semantic segmentation,” in *Proceedings of the IEEE conference on computer vision and pattern recognition*, pp. 3431–3440, 2015.
- [2] O. Ronneberger, P. Fischer, and T. Brox, “U-Net: Convolutional networks for biomedical image segmentation,” in *Medical Image Computing and Computer-Assisted Intervention—MICCAI 2015: 18th International Conference, Munich, Germany, October 5–9, 2015, Proceedings, Part III 18*, pp. 234–241, Springer, 2015.

- [3] F. Milletari, N. Navab, and S.-A. Ahmadi, "V-Net: Fully convolutional neural networks for volumetric medical image segmentation," in *2016 fourth international conference on 3D vision (3DV)*, pp. 565–571, Ieee, 2016.
- [4] C. You, Y. Zhou, R. Zhao, L. Staib, and J. S. Duncan, "SimCVD: Simple contrastive voxel-wise representation distillation for semi-supervised medical image segmentation," *IEEE Transactions on Medical Imaging*, vol. 41, no. 9, pp. 2228–2237, 2022.
- [5] S. Laine and T. Aila, "Temporal ensembling for semi-supervised learning," *arXiv preprint arXiv:1610.02242*, 2016.
- [6] A. Tarvainen and H. Valpola, "Mean teachers are better role models: Weight-averaged consistency targets improve semi-supervised deep learning results," *Advances in neural information processing systems*, vol. 30, 2017.
- [7] M. Sajjadi, M. Javanmardi, and T. Tasdizen, "Regularization with stochastic transformations and perturbations for deep semi-supervised learning," *Advances in neural information processing systems*, vol. 29, 2016.
- [8] M. Abdar, F. Pourpanah, S. Hussain, D. Rezazadegan, L. Liu, M. Ghavamzadeh, P. Fieguth, X. Cao, A. Khosravi, U. R. Acharya, et al., "A review of uncertainty quantification in deep learning: Techniques, applications and challenges," *Information Fusion*, vol. 76, pp. 243–297, 2021.
- [9] D. Berthelot, N. Carlini, I. Goodfellow, N. Papernot, A. Oliver, and C. A. Raffel, "MixMatch: A holistic approach to semi-supervised learning," *Advances in neural information processing systems*, vol. 32, 2019.
- [10] J. Chen, Z. Yang, and D. Yang, "MixText: Linguistically-informed interpolation of hidden space for semi-supervised text classification," *arXiv preprint arXiv:2004.12239*, 2020.
- [11] D.-H. Lee et al., "Pseudo-label: The simple and efficient semi-supervised learning method for deep neural networks," in *Workshop on challenges in representation learning, ICML*, vol. 3, p. 896, 2013.
- [12] M. N. Rizve, K. Duarte, Y. S. Rawat, and M. Shah, "In defense of pseudo-labeling: An uncertainty-aware pseudo-label selection framework for semi-supervised learning," *arXiv preprint arXiv:2101.06329*, 2021.
- [13] P. Cascante-Bonilla, F. Tan, Y. Qi, and V. Ordonez, "Curriculum labeling: Revisiting pseudo-labeling for semi-supervised learning," 2020.
- [14] X. Zhao, Z. Qi, S. Wang, Q. Wang, X. Wu, Y. Mao, and L. Zhang, "RCPS: Rectified contrastive pseudo supervision for semi-supervised medical image segmentation," *arXiv preprint arXiv:2301.05500*, 2023.
- [15] H. Zhang, M. Cisse, Y. N. Dauphin, and D. Lopez-Paz, "mixup: Beyond empirical risk minimization," in *International Conference on Learning Representations*, 2018.
- [16] F. Isensee, P. F. Jäger, S. A. Kohl, J. Petersen, and K. H. Maier-Hein, "Automated design of deep learning methods for biomedical image segmentation," *arXiv preprint arXiv:1904.08128*, 2019.
- [17] J. Xu, M. Li, and Z. Zhu, "Automatic data augmentation for 3D medical image segmentation," in *Medical Image Computing and Computer Assisted Intervention–MICCAI 2020: 23rd International Conference, Lima, Peru, October 4–8, 2020, Proceedings, Part I 23*, pp. 378–387, Springer, 2020.
- [18] Z. Gu, J. Cheng, H. Fu, K. Zhou, H. Hao, Y. Zhao, T. Zhang, S. Gao, and J. Liu, "CE-Net: Context encoder network for 2D medical image segmentation," *IEEE transactions on medical imaging*, vol. 38, no. 10, pp. 2281–2292, 2019.
- [19] Z. Liu, Y. Lin, Y. Cao, H. Hu, Y. Wei, Z. Zhang, S. Lin, and B. Guo, "Swin transformer: Hierarchical vision transformer using shifted windows," in *Proceedings of the IEEE/CVF international conference on computer vision*, pp. 10012–10022, 2021.
- [20] H. Cao, Y. Wang, J. Chen, D. Jiang, X. Zhang, Q. Tian, and M. Wang, "Swin-Unet: Unet-like pure transformer for medical image segmentation," in *European conference on computer vision*, pp. 205–218, Springer, 2022.
- [21] H. Kervade, J. Bouchtiba, C. Desrosiers, E. Granger, J. Dolz, and I. B. Ayed, "Boundary loss for highly unbalanced segmentation," *Medical image analysis*, vol. 67, p. 101851, 2021.
- [22] A. Vaswani, N. Shazeer, N. Parmar, J. Uszkoreit, L. Jones, A. N. Gomez, Ł. Kaiser, and I. Polosukhin, "Attention is all you need," *Advances in neural information processing systems*, vol. 30, 2017.
- [23] S. Li, C. Zhang, and X. He, "Shape-aware semi-supervised 3D semantic segmentation for medical images," in *Medical Image Computing and Computer Assisted Intervention–MICCAI 2020: 23rd International Conference, Lima, Peru, October 4–8, 2020, Proceedings, Part I 23*, pp. 552–561, Springer, 2020.
- [24] X. Luo, J. Chen, T. Song, and G. Wang, "Semi-supervised medical image segmentation through dual-task consistency," in *Proceedings of the AAAI Conference on Artificial Intelligence*, vol. 35, pp. 8801–8809, 2021.
- [25] X. Luo, G. Wang, W. Liao, J. Chen, T. Song, Y. Chen, S. Zhang, D. N. Metaxas, and S. Zhang, "Semi-supervised medical image segmentation via uncertainty rectified pyramid consistency," *Medical Image Analysis*, vol. 80, p. 102517, 2022.
- [26] L. Yu, S. Wang, X. Li, C.-W. Fu, and P.-A. Heng, "Uncertainty-aware self-ensembling model for semi-supervised 3d left atrium segmentation," in *Medical Image Computing and Computer Assisted Intervention–MICCAI 2019: 22nd International Conference, Shenzhen, China, October 13–17, 2019, Proceedings, Part II 22*, pp. 605–613, Springer, 2019.
- [27] X. Li, L. Yu, H. Chen, C.-W. Fu, L. Xing, and P.-A. Heng, "Transformation-consistent self-ensembling model for semisupervised medical image segmentation," *IEEE Transactions on Neural Networks and Learning Systems*, vol. 32, no. 2, pp. 523–534, 2020.
- [28] W. Hang, W. Feng, S. Liang, L. Yu, Q. Wang, K.-S. Choi, and J. Qin, "Local and global structure-aware entropy regularized mean teacher model for 3D left atrium segmentation," in *Medical Image Computing and Computer Assisted Intervention–MICCAI 2020: 23rd International Conference, Lima, Peru, October 4–8, 2020, Proceedings, Part I 23*, pp. 562–571, Springer, 2020.
- [29] Y. Wu, Z. Ge, D. Zhang, M. Xu, L. Zhang, Y. Xia, and J. Cai, "Mutual consistency learning for semi-supervised medical image segmentation," *Medical Image Analysis*, vol. 81, p. 102530, 2022.
- [30] R. Wang, Y. Wu, H. Chen, L. Wang, and D. Meng, "Neighbor matching for semi-supervised learning," in *Medical Image Computing and Computer Assisted Intervention–MICCAI 2021: 24th International Conference, Strasbourg, France, September 27–October 1, 2021, Proceedings, Part II 24*, pp. 439–449, Springer, 2021.
- [31] C. Li, L. Dong, Q. Dou, F. Lin, K. Zhang, Z. Feng, W. Si, X. Deng, Z. Deng, and P.-A. Heng, "Self-ensembling co-training framework for semi-supervised covid-19 CT segmentation," *IEEE Journal of Biomedical and Health Informatics*, vol. 25, no. 11, pp. 4140–4151, 2021.
- [32] K. Clark, B. Vendt, K. Smith, J. Freymann, J. Kirby, P. Koppel, S. Moore, S. Phillips, D. Maffitt, M. Pringle, et al., "The cancer imaging archive (TCIA): maintaining and operating a public information repository," *Journal of digital imaging*, vol. 26, pp. 1045–1057, 2013.
- [33] Z. Xiong, Q. Xia, Z. Hu, N. Huang, C. Bian, Y. Zheng, S. Vesal, N. Ravikumar, A. Maier, X. Yang, et al., "A global benchmark of algorithms for segmenting the left atrium from late gadolinium-enhanced cardiac magnetic resonance imaging," *Medical image analysis*, vol. 67, p. 101832, 2021.
- [34] O. Bernard, A. Lalonde, C. Zotti, F. Cervenansky, X. Yang, P.-A. Heng, I. Cetin, K. Lekadir, O. Camara, M. A. G. Ballester, et al., "Deep learning techniques for automatic MRI cardiac multi-structures segmentation and diagnosis: is the problem solved?," *IEEE transactions on medical imaging*, vol. 37, no. 11, pp. 2514–2525, 2018.
- [35] Y. Wu, Z. Wu, Q. Wu, Z. Ge, and J. Cai, "Exploring smoothness and class-separation for semi-supervised medical image segmentation," in *International Conference on Medical Image Computing and Computer Assisted Intervention*, pp. 34–43, Springer, 2022.
- [36] I. Goodfellow, J. Pouget-Abadie, M. Mirza, B. Xu, D. Warde-Farley, S. Ozair, A. Courville, and Y. Bengio, "Generative adversarial nets," *Advances in neural information processing systems*, vol. 27, 2014.
- [37] M. Ren, E. Triantafillou, S. Ravi, J. Snell, K. Swersky, J. B. Tenenbaum, H. Larochelle, and R. S. Zemel, "Meta-learning for semi-supervised few-shot classification," *arXiv preprint arXiv:1803.00676*, 2018.